

Influences of double diffusion upon radiative flow of thin film Maxwell fluid through a stretching channel

Arshad Khan, Ishtiaq Ali, Musawa Yahya Almusawa, Taza Gul, and Wajdi Alghamdi

Citation: Chin. Phys. B, 2023, 32 (**8**): 084401. DOI: 10.1088/1674-1056/acc059
Journal homepage: http://cpb.iphy.ac.cn; http://iopscience.iop.org/cpb

What follows is a list of articles you may be interested in

Thermal rectification induced by Wenzel-Cassie wetting state transition on nano-structured solid-liquid interfaces

Haiyang Li(李海洋), Jun Wang(王军), and Guodong Xia(夏国栋)
Chin. Phys. B, 2023, 32 (**5**): 054401. DOI: 10.1088/1674-1056/aca9c1

Uniformity principle of temperature difference field in heat transfer optimization

Xue-Tao Cheng(程雪涛), Xin-Gang Liang(梁新刚)
Chin. Phys. B, 2019, 28 (**6**): 064402. DOI: 10.1088/1674-1056/28/6/064402

Three-dimensional human thermoregulation model based on pulsatile blood flow and heating mechanism

Si-Na Dang(党思娜), Hong-Jun Xue(薛红军), Xiao-Yan Zhang(张晓燕), Jue Qu(瞿珏), Cheng-Wen Zhong(钟诚文), Si-Yu Chen(陈思宇)
Chin. Phys. B, 2018, 27 (**11**): 114402. DOI: 10.1088/1674-1056/27/11/114402

Simulation on effect of metal/graphene hybrid transparent electrode on characteristics of GaN light emitting diodes

Ming-Can Qian(钱明灿), Shu-Fang Zhang(张淑芳), Hai-Jun Luo(罗海军), Xing-Ming Long(龙兴明), Fang Wu(吴芳), Liang Fang(方亮), Da-Peng Wei(魏大鹏), Fan-Ming Meng(孟凡明), Bao-Shan Hu(胡宝山)
Chin. Phys. B, 2017, 26 (**10**): 104402. DOI: 10.1088/1674-1056/26/10/104402

Influences of double diffusion upon radiative flow of thin film Maxwell fluid through a stretching channel

Arshad Khan[1,†], Ishtiaq Ali[2], Musawa Yahya Almusawa[3], Taza Gul[4], and Wajdi Alghamdi[5]

[1] *College of Aeronautical Engineering, National University of Sciences and Technology (NUST), Sector H-12, Islamabad* 44000, *Pakistan*
[2] *Department of Mathematics and Statistics, College of Science, King Faisal University, Al-Ahsa* 31982, *Saudi Arabia*
[3] *Department of Mathematics, Faculty of Science, Jazan University, Jazan, Saudi Arabia*
[4] *Department of Mathematics, City University of Science and Information Technology, Peshawar* 25000, *Pakistan*
[5] *Department of Information Technology, Faculty of Computing and Information Technology, King Abdulaziz University, Jeddah* 80261, *Saudi Arabia*

(Received 2 November 2022; revised manuscript received 4 February 2023; accepted manuscript online 2 March 2023)

This work explores the influence of double diffusion over thermally radiative flow of thin film hybrid nanofluid and irreversibility generation through a stretching channel. The nanoparticles of silver and alumina have mixed in the Maxwell fluid (base fluid). Magnetic field influence has been employed to channel in normal direction. Equations that are going to administer the fluid flow have been converted to dimension-free notations by using appropriate variables. Homotopy analysis method is used for the solution of the resultant equations. In this investigation it has pointed out that motion of fluid has declined with growth in magnetic effects, thin film thickness, and unsteadiness factor. Temperature of fluid has grown up with upsurge in Brownian motion, radiation factor, and thermophoresis effects, while it has declined with greater values of thermal Maxwell factor and thickness factor of the thin film. Concentration distribution has grown up with higher values of thermophoresis effects and has declined for augmentation in Brownian motion.

Keywords: Maxwell fluid flow, magnetohydrodynamic (MHD), hybrid nano fluid flow, stretching channel, double diffusion, entropy generation, HAM technique

PACS: 44.90.+c, 47.35.–I, 05.40.Jc, 47.15.gm **DOI:** 10.1088/1674-1056/acc059

1. Introduction

Thin film plays a dynamic role in quantum phenomena in super-lattices and multi ferric materials. When the base fluids include nanoparticles thin films are more suitable for analyzing the process of thermal flow. Qasim *et al.*[1] investigated the heat and mass flows by using thin film nanoparticles-based fluid over a stretching surface and concluded that temperature of fluid decreases with the values of nanoparticles volume fraction and viscous dissipation factor increasing. Adebayo *et al.*[2] studied pulsed wave experimentally by using thin film flow past a plate and numerically solved their problem. Akkus *et al.*[3] considered a thin film flow of fluid and analyzed the modeled equations numerically. Dantapat *et al.*[4] studied thin film flow solution analytically by employing viscous fluid flow past a stretching sheet. Saeed *et al.*[5] debated on nonlinear convection fluid flow for thin film nanofluid past an inclined plate and analyzed the growth of mass and thermal flow rate in the form of percentage values.

In recent years, the explorations linked to fluid of non-Newtonian nature have received much attention due to its engineering and industrial applications in making metallic plates and fabricating rolling sheets and plastic polymers. Such a fluid cannot be described by using a single constitutive equation; but they are described by many equations. Such fluids also involve Maxwell fluid equations. Islam *et al.*[6] inspected mixed convective and thermally radiative Maxwell nanofluid flow on horizontally placed stretching cylinder by using the effects of heat sink/source upon flow system. Nadeem *et al.*[7] discussed Maxwell nanofluid flow past an expanding surface and noticed that the temperature distribution increases with nanoparticles concentration growing. The influence of thermal radiation was employed by Zainal *et al.*[8] for investigating Maxwell nanofluid past a shrinking surface. Jawad *et al.*[9] have studied analytically the mixed convective MHD Maxwell nanofluid flow subjected to Dufour, Soret and thermal conductivity effects. Abdal *et al.*[10] explored MHD Maxwell nanofluid flow over a stretched and permeable surface subjected to activation energy and bioconvection effects. Abbasi and Shehzad[11] have analyzed threedimensional Maxwell fluid flow past a bidirectional stretched sheet.

The discipline for studying the characteristics of electrically conducted fluid such as salty water, is termed magnetohydrodynamics (MHD). The MHD has many applications in engineering and medical industry,[12] for instance magnetic endoscopy, treatment of cancer tumor, and drug targeting. Turkyilmazoglu[13] analyzed the thermal flow past a rotary disk by applying a uniform magnetic field in the horizontal direction and has concluded numerically that thermal profile is amplified with magnetic factor increasing. Saleh and Hashim[14] discussed MHD mixed convective fully developed

†Corresponding author. E-mail: arshad8084@gmail.com
© 2023 Chinese Physical Society and IOP Publishing Ltd

flow through a vertical channel and highlighted that reversal flow also exists in the channel. In Ref. [15], the authors studied the transport characteristics for n-type diluted magnetic semi-conductors by using the properties of electronic and magnetic effects. Uddin *et al.*[16] discussed intelligent network for MHD double diffusive thin liquid flow past a stretched surface. Hosseinzadeh *et al.*[17] discussed MHD micro-polar hybrid nanofluid flowing through a sinusoidal cylinder and determined that the velocity is weakened and temperature as well as skin frictionincreases with intensification in concentration of nanoparticles and magnetic field effect. Guedri *et al.*[18] investigated the dissipative flow and generation of irreversibility for EMHD fluid flow on a surface, and revealed that temperature increases with electric field effect and magnetic field effect increasing.

It is noticed that in modern time technology the thermal conductance of many base fluids needs to be improved. For this purpose, nanoparticles are mixed in a pure fluid and the resulting fluid is termed nanofluid. The nanofluid has greater thermal conductivity than normal fluids. Such a fluid has many industrial applications, such as coolant of exchangers, electric devices and automobile engine. The idea of mixing nanoparticles into pure fluid was first introduced by Choi and Eastman[19] for maximizing the thermal conductance of normal fluid. Najafabadi *et al.*[20] discussed nanofluid flow through a vertically placed channel under polynomial boundary conditions. Ghadikolaei *et al.*[21] studied the MHD Casson nanoparticles flow past an inclined stretched surface and deduced that the fluid motion declines with magnetic factor increasing. Shah *et al.*[22] have carried out a novel work by considering gold nanoparticles in blood flowing through a permeable channel subjected to micro-polar effects and thermal radiations. Khan *et al.*[23] discussed the radiative rotary flow for MHD Casson nanofluid over a spinning cylinder with influence of Joule heating dissipation. Bilal *et al.*[24] analyzed numerically the time-based hybrid nanofluid flow by using chemically activated energy and deduced that the fluid motion and thermal distribution were augmented by employing hybrid nanoparticles. Rajput *et al.*[25] inspected the augmentation of Nusselt number for nanofluid in heat exchanger by considering CNT and copper-oxide in flow system.

The production of entropy in the fluid flow phenomenon is pretty important and more applicable concept. It is produced because of irreversibility in the flow system. To enhance the effectiveness of the system, entropy needs minimizing. Ullah *et al.*[26] discussed the production of entropy carried out the thermal flow analysis in power law fluid motion and highlighted that with the increase of Eckert number the production of entropy augments while Bejan number decreases. Butt and Ali[27] analyzed the influence of magnetic field on the production of irreversibility for fluid flow on an elongated surface. Cheng and Liang[28] analyzed the constraints on the production of entropy for parallel two-stream flow thermal exchangers using the viscous heating effect and deduced that the minimization of resistance to entropy causes the thermal flow of fluid to augment. Khan *et al.*[29] investigated the thermal flow and production of irreversibility for MHD Casson nanofluid flow over a spinning cylinder.

Any physical phenomenon when it is modeled mathematically, mostly leads to some nonlinear differential equations. The nonlinearity of such equations is much high in some physical problems. The analytical solving of such modeled equations is very difficult even impossible sometimes. Researchers have settled many procedures to handle such nonlinear problems mathematically. Homotopy analysis method[30] is one of such techniques used to solve various nonlinear problems.

Considered in this work are the following iteams.

(i) Effects of double diffusion on thermally radiative flow of thin film hybrid nanofluid through a stretching channel.

(ii) Irreversibility produced by a flow system consisting of Maxwell hybrid nanofluid.

(iii) Maxwell fluid is taken as pure fluid while Ag and TiO_2 nanoparticles suspend in it to hybridize the pure fluid.

(iv) Magnetic effects are applied in the normal direction to current flow problem.

2. Formulation of problem

A thin film flow of fluid is considered through a stretching channel subjected to the influence of thermal radiations. The motion in fluid is induced by applying a force to a sheet that starts motion due to stretched behavior of the surface (as shown in Fig. 1). The quantity $h(t)$ describes the width of the sheet. The initial velocity of the fluid is assumed to be zero so that the fluid motion is systematically established due to motion of sheet. Figure 1 shows the graphical view of flow problem.

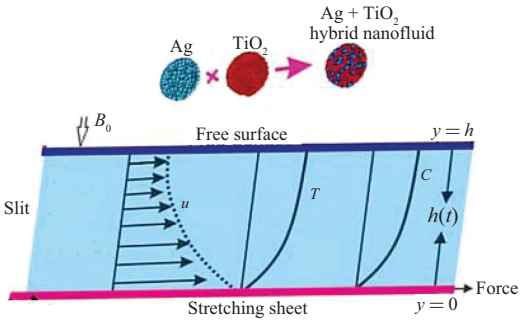


Fig. 1. Physical geometry of flow problem.

The motion of sheet in the presence of force is given by

$$U = \frac{bx}{(1-\alpha t)^{1/2}}, \tag{1}$$

where U represents the velocity along the x axis while elasticity term is given by $b/(1-\alpha t)^{1/2}$ with $\alpha \geq 0$ but $\alpha < 1$ as

time increases. The T_0, T_r and C_0, C_r are the reference temperatures and concentrations respectively, and they are in the following order: $T_0 \geq T_r \geq 0$ and $C_0 \geq C_r \geq 0$. Moreover, the surface temperature of sheet is depicted by T_s. The magnetic field in the transverse direction is given by the following expression:

$$B_0(t,x) = \frac{B_0}{(1-\alpha t)^{1/2}}. \tag{2}$$

The leading equations are modeled as[1,5,31]

$$\frac{\partial u}{\partial x} + \frac{\partial v}{\partial y} = 0, \tag{3}$$

$$\left(\frac{\partial u}{\partial t} + v\frac{\partial u}{\partial y} + u\frac{\partial u}{\partial x}\right) + \lambda_1\left(v^2\frac{\partial^2 u}{\partial y^2} + 2uv\frac{\partial^2 u}{\partial x\,\partial y} + u^2\frac{\partial^2 u}{\partial x^2}\right) = \upsilon\frac{\partial^2 u}{\partial y^2} - \frac{\sigma B_0^2}{\rho}\left(u + \lambda_1 v\frac{\partial u}{\partial y}\right), \tag{4}$$

$$\begin{aligned}\frac{\partial T}{\partial t} + u\frac{\partial T}{\partial x} + v\frac{\partial T}{\partial y} &= \alpha\left[\frac{\partial^2 T}{\partial y^2}\right] + \tau\left[D_B\left(\frac{\partial C}{\partial y}\right)\left(\frac{\partial T}{\partial y}\right) + \frac{D_T}{T_h}\left(\frac{\partial T}{\partial y}\right)^2\right] \\ &+ \lambda_2\left[\begin{array}{l}\dfrac{\partial^2 T}{\partial t^2} + u\dfrac{\partial u}{\partial x}\dfrac{\partial T}{\partial x} + v\dfrac{\partial v}{\partial y}\dfrac{\partial T}{\partial y} + u\dfrac{\partial v}{\partial x}\dfrac{\partial T}{\partial y} + v\dfrac{\partial u}{\partial x}\dfrac{\partial T}{\partial x} \\ +2u\dfrac{\partial^2 T}{\partial x\partial t} + \dfrac{\partial T}{\partial x}\dfrac{\partial u}{\partial t} + 2v\dfrac{\partial^2 T}{\partial y\partial t} + \dfrac{\partial T}{\partial t}\dfrac{\partial v}{\partial t} + u^2\dfrac{\partial^2 T}{\partial x^2} + v^2\dfrac{\partial^2 T}{\partial y^2} + 2uv\dfrac{\partial^2 T}{\partial x\partial y}\end{array}\right],\end{aligned} \tag{5}$$

$$\begin{aligned}\frac{\partial C}{\partial t} + v\frac{\partial C}{\partial y} + u\frac{\partial C}{\partial x} &= \frac{D_T}{T_h}\frac{\partial^2 T}{\partial y^2} + D_{Bhnf}\frac{\partial^2 C}{\partial y^2} \\ &+ \lambda_3\left[\begin{array}{l}\dfrac{\partial^2 C}{\partial t^2} + u\dfrac{\partial C}{\partial x}\dfrac{\partial u}{\partial x} + v\dfrac{\partial C}{\partial y}\dfrac{\partial v}{\partial y} + u\dfrac{\partial C}{\partial y}\dfrac{\partial v}{\partial x} + v\dfrac{\partial C}{\partial x}\dfrac{\partial u}{\partial x} \\ +2u\dfrac{\partial^2 C}{\partial x\partial t} + \dfrac{\partial C}{\partial x}\dfrac{\partial u}{\partial t} + 2v\dfrac{\partial^2 C}{\partial y\partial t} + \dfrac{\partial C}{\partial t}\dfrac{\partial v}{\partial t} + u^2\dfrac{\partial^2 C}{\partial x^2} + v^2\dfrac{\partial^2 C}{\partial y^2} + 2uv\dfrac{\partial^2 C}{\partial x\partial y}\end{array}\right].\end{aligned} \tag{6}$$

The flow components along the coordinate axes are u, v, while the density, thermal conductivity, specific heat, and viscosity are denoted by ρ, K, C_p, and μ.

The conditions at boundaries are given below:

$$\begin{aligned}&u = U_w,\ \ v = 0,\ \ C = C_w,\ \ T = T_w,\quad \text{when } y = 0,\\ &\frac{\partial u}{\partial y}(\mu) = \frac{\partial C}{\partial y} = \frac{\partial T}{\partial y} = 0,\ \ v = \frac{\partial h}{\partial t},\quad \text{when } y = h(t).\end{aligned} \tag{7}$$

Given below are the similarity variables which are used for transformation:

$$\begin{aligned}&\psi(x,y,t) = \left(\frac{b\upsilon}{1-\alpha t}\right)^{0.5} x f(\zeta),\ \ C(x,y,t) = C_0 - C_r(1-\alpha t)^{-1.5}\left(\frac{bx^2}{2\upsilon}\right)\varphi(\zeta),\\ &T(x,y,t) = T_0 - T_r(1-\alpha t)^{-1.5}\left(\frac{bx^2}{2\upsilon}\right)\theta(\zeta),\quad \zeta = \left(\frac{b}{\upsilon(1-\alpha t)}\right)^{0.5} y.\end{aligned} \tag{8}$$

The thickness of the thin film is described as

$$\beta = h(t)\left(b/\upsilon(1-\alpha t)\right)^{0.5}, \tag{9}$$

$$\frac{\mathrm{d}h}{\mathrm{d}t} = \frac{\alpha\beta}{2}(1-\alpha t)^{-0.5}\left(\frac{\upsilon}{b}\right)^{0.5}. \tag{10}$$

Using Eq. (8) the following equations are obtained:

$$f''' - (f')^2 + f''f - \lambda\left(f^2 f''' - 2ff''f'\right) - S\left(f' + \frac{\zeta}{2}f''\right) + M\left(\lambda ff'' - f'\right) = 0, \tag{11}$$

$$\begin{aligned}&\frac{1}{Pr}\Theta'' - \frac{S}{2}\left(3\Theta + \eta\Theta'\right) - 2f'\Theta + f\Theta' + N_b\Phi'\Theta' + Nt\left(\Theta'\right)^2 \\ &+ \lambda_T\left[\begin{array}{l}\dfrac{3S^2}{2}\left(\Theta + \Theta' + \dfrac{\eta}{2}\Theta''\right) - ff'\Theta + ff'\Theta' + 2(f')^2\Theta + Sf'(3\Theta' + \eta\Theta'') \\ +2S\Theta\left(f' + \dfrac{\eta}{2}f''\right) - 2Sf\left(2\Theta' + \dfrac{\eta}{2}\Theta''\right) - \dfrac{S^2}{4}(f + \eta f')(3\Theta + \eta\Theta') \\ +f^2\Theta'' - Sff'(3\Theta' + \eta\Theta'')\end{array}\right] = 0,\end{aligned} \tag{12}$$

$$\Phi''+S_{\rm c}\left(\frac{S}{2}\left(3\Phi+\eta\Phi'\right)-2f'\Phi+f\Phi'\right)+\frac{N_{\rm t}}{N_{\rm b}}\Theta''$$
$$+\lambda_{\rm C}\begin{bmatrix}\frac{3S^2}{2}\left(\Phi+\Phi'+\frac{\eta}{2}\Phi''\right)+2\left(f'\right)^2\Phi+ff'\Phi'-ff'\Phi+Sf'\left(3\Phi'+\eta\Phi''\right)\\+2S\Phi\left(f'+\frac{\eta}{2}f''\right)-2Sf\left(2\Phi'+\frac{\eta}{2}\Phi''\right)-\frac{S^2}{4}\left(f+\eta f'\right)\left(3\Phi+\eta\Phi'\right)\\+f^2\Phi''-Sff'\left(3\Phi'+\eta\Phi''\right)\end{bmatrix}=0. \tag{13}$$

Here, the Prandtl number, Brownian, unsteadiness, magnetic, Maxwell, and thermophoresis factors are presented by Pr, $N_{\rm b}$, S, M, λ, $N_{\rm t}$ specifically, they are given by the following mathematical expression:

$$S=\frac{\alpha}{b},\ N_{\rm b}=\frac{\tau D_{\rm B}\left(C_{\rm w}-C_{\infty}\right)}{\upsilon},\ \lambda_{\rm T}=\frac{\lambda_1}{(1-\alpha t)},\ N_{\rm t}=\frac{\tau D_{\rm T}\left(T_{\rm w}-T_{\infty}\right)}{\upsilon T_{\rm h}},\ \lambda_{\rm C}=\frac{\lambda_2}{(1-\alpha t)},\ M=\frac{\sigma B_0^2}{\rho b},\ Pr=\frac{\mu C_{\rm p}}{k}. \tag{14}$$

The subjected boundary conditions are converted into the following form by substituting Eq. (8) into Eq. (7):

$$f(0)=0,\quad f(\beta)=\frac{\beta S}{2},\quad f'(0)=1,\quad f''(\beta)=0,\quad \Theta'(\beta)=0,\quad \Theta(0)=1,\quad \Phi(0)=1,\quad \Phi'(\beta)=0. \tag{15}$$

2.1. Quantities of interest

Some important quantities of interest are defined by the following mathematical expressions:

Skin friction

$$C_{\rm f}=\frac{2\tau_{\rm w}}{\rho U_{\rm w}^2},$$

Nusselt number

$$N_{\rm u}=\frac{q_{\rm w}x}{k(T_{\rm w}-T_0)}, \tag{16}$$

Sherwood number

$$S_{\rm n}=\frac{q_{\rm m}x}{\left(C_{\rm w}-C_0\right)D_{\rm B}},$$

with

$$\tau_{\rm w}=\mu\left(\frac{\partial u}{\partial y}\right)\Big|_{y=0},$$

$$q_{\rm m}=-D_{\rm B}\left(\frac{\partial C}{\partial y}\right)\Big|_{y=0},$$
$$q_{\rm w}=-k\left(\frac{\partial T}{\partial y}\right)\Big|_{y=0}. \tag{17}$$

In dimensionless notations we have

$$Re^{1/2}C_{\rm f}=-f''(0),\quad Re^{-1/2}N_{\rm u}=-\Theta'(0),$$
$$Re^{-1/2}S_{\rm h}=-\Phi'(0),\quad Re=\frac{xU_{\rm w}}{\upsilon}. \tag{18}$$

2.2. Entropy rate

The production of entropy is a basic concept and plays a major part in any engineering or physical phenomenon. It is based on second thermodynamics law which states that irreversibility is an increasing phenomenon in an isolated system through some activations. Its mathematical expression is given by

$$S_{\rm g}=\frac{k}{T_{\infty}^2}\left(\frac{\partial T}{\partial y}\right)^2+\frac{\mu}{T_{\infty}}\left(\frac{\partial u}{\partial y}\right)^2+\frac{\mu}{T_{\infty}K}(u)^2+\frac{R_{\rm D}}{C_{\infty}}\left(\frac{\partial C}{\partial y}\right)^2+\frac{R_{\rm D}}{T_{\infty}}\frac{\partial C}{\partial y}\frac{\partial T}{\partial y},$$
$$S_{\rm G}=(1+R_{\rm d})\lambda\left(\Theta'\right)^2+PrE_{\rm c}\left[\left(f''\right)^2+\lambda r\left(f'\right)^2+L\left(\Theta'\Phi'+\left(\Phi'\right)^2\right)\right]. \tag{19}$$

Here $S_{\rm G}=S_{\rm g}T_{\infty}/(T_{\rm w}-T_{\infty})$ is the entropy production rate, $L=R_{\rm D}\left(C_{\rm w}-C_{\infty}\right)/k_{\rm f}$ is the diffusive factor, and $\lambda=(T_{\rm w}-T_{\infty})/T_{\infty}$ is the thermal difference factor.

2.3. Bejan number

The mathematical expression for Bejan number is given as follows:

$$B_{\rm e}=\frac{\lambda\left(\Theta'\right)^2}{\lambda\left(\Theta'\right)^2+{\rm Pr}E_{\rm c}\left[\left(f''\right)^2+\lambda r\left(f'\right)^2+L\left(\Theta'\Phi'+\left(\Phi'\right)^2\right)\right]}. \tag{20}$$

3. Solution method

To solve Eqs. (11)–(3) with the help of Eq. (15), HAM code[29] is used as a method of solution. This method is quite fruitful for the evaluation of highly nonlinear equations and ensures the solution convergence as well. The starting presumption in current

investigation is defined as follows:

$$f_0(\eta)=\frac{3}{2\beta^2}(2-S)\left[\frac{\eta^3}{6}-\frac{\beta\eta^2}{2}\right]+\eta,\quad \theta_0(\eta)=1,\quad \varphi_0(\eta)=1, \tag{21}$$

with

$$L_f(f)=A_1\frac{\eta^3}{6}+A_2\frac{\eta^2}{2}+A_3\eta+A_4,\ L_\theta(\theta)=B_1\eta+B_2,\ L_\varphi(\varphi)=C_1\eta+C_2. \tag{22}$$

Further details can be seen in Ref. [32].

4. Discussion of results

In this problem the governing equations are converted **in**to dimension-free notations by employing a suitable set of variables. Homotopy analysis method has been used for the solving the resulting equations. The effect of emerging factors on flow profiles has deliberated in following subsections.

4.1. Velocity profiles

Figures 2–4 show the influences of different substantial factors on fluid motion. Figure 2 exhibits the influence of unsteadiness parameter S on fluid motion where the growing of S results in the increase of the values of velocity characteristics. It can be explained by the fact that with the growing of S, the width of momentum boundary layer diminishes for greater values of thickness of film (*i.e.* $\beta=0.70, 0.71, 0.72, 0.73$), thus the stretching performance of the surface finally reduces the fluid's motion as depicted in Fig. 2.

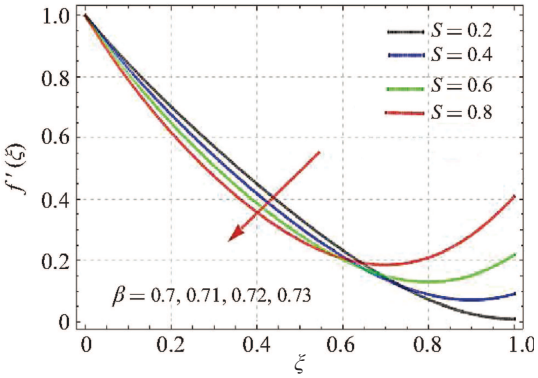


Fig. 2. Variations of f' with ζ for different values of β and S.

It can be observed in Fig. 3 that the growing of film thickness β is responsible for decay in the fluid motion for $\zeta=0.1$–0.8. Actually, for increased values of β, maximum confrontation is realized by motion of fluid that reduces the strength of boundary layer of momentum and eventually retards the velocity characteristics. Higher values of M reduce the fluid's velocity for progression in β. It can be explained by the fact that growing value of magnetic factor yields Lorentz force in the reverse direction of motion of fluid, therefore the fluid particles experience a resistance for $\beta=0.70, 0.72, 0.74, 0.76$. In this process the fluid motion decays as shown in Fig. 4.

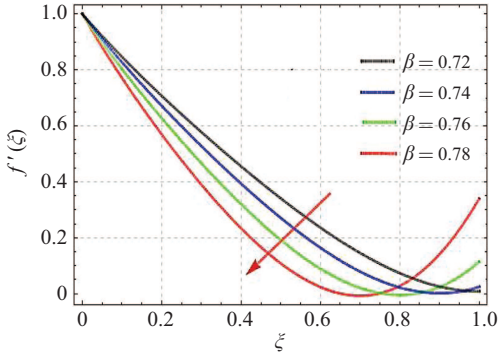


Fig. 3. Variations of f' with ζ for different values of β.

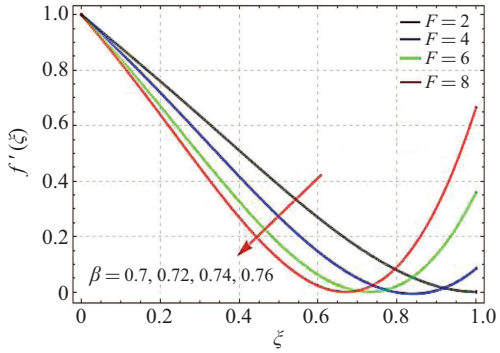


Fig. 4. Variations of f' with ζ for different values of F and β.

4.2. Temperature profiles

The influences of different factors on temperature are presented in Figs. 5–9 for different values of film thickness β, *i.e.*, $\beta=0.54, 0.55, 0.56, 0,57$. When there is an increase in the values of Brownian factor N_b, more collisions among the nanoparticles take place, in this process the maximum amount of kinetic energy is shifted toward thermal energy. In this process the strength of temperature layer is enhanced supplementing the thermal distribution of Maxwell fluid as portrayed in Fig. 5. The influence of thermophore factor N_t on thermal profile is shown in Fig. 6. Since $N_t=\tau D_T(T_w-T_\infty)/\upsilon T_h$, with the growing of N_t the temperature gradient augments, therefore maximum heat flows from warmer zone to colder zone Because of this phenomenon the temperature of Maxwell nanofluid augments as depicted in Fig. 6. A growth in unsteadiness factor S causes an upsurge in temperature characteristics as shown in Fig. 7. Actually, the growing of S depicts the rate of heating over cooling rate due to which more transporta-

tion of heat occurs. Hence, thermal profiles increase for growing values of S as given in Fig. 7. A progression in Maxwell parameter λ_T results in a decline in thermal flow profiles as described in Fig. 8. Essentially, the upsurge in λ_T reduces the heat diffusivity and deteriorates the thermal boundary layer width due to which a smaller amount of heat transmission is ensured, which substantiates the lessening of temperature.

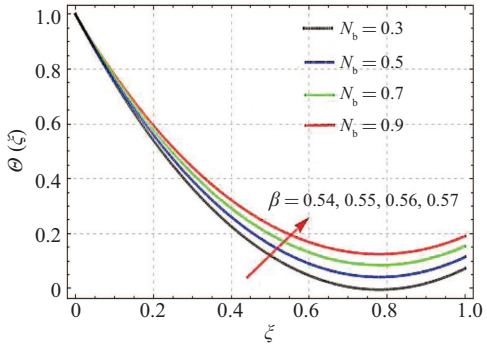


Fig. 5. Thermal profiles for different values of β and N_b.

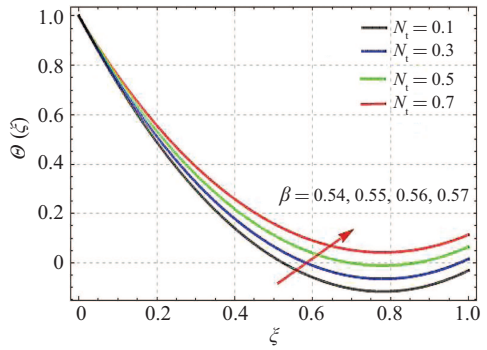


Fig. 6. Thermal profiles for different values of β and N_t.

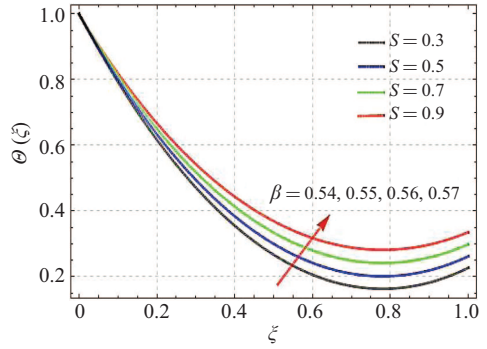


Fig. 7. Thermal profiles for different values of β and S.

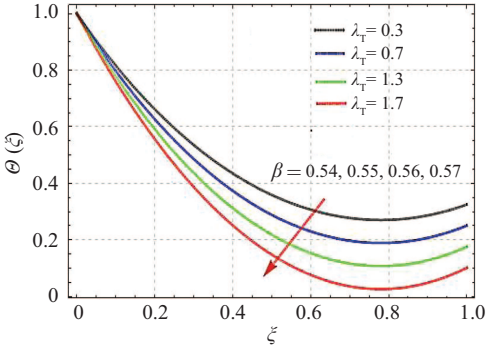


Fig. 8. Thermal profiles for different values of β and λ_T.

4.3. Concentration profiles

The effects of different factors on concentration are shown in Figs. 9–12. It is noticed from Fig. 9 that concentration of Maxwell nanofluid has retarded with the growing of Brownian motion factor N_b when $\beta = 0.6, 0.7, 0.8, 0.9$. Actually, when N_b augments more friction to fluid motion is produced, therefore less mass diffuses with the further growing of heat diffusion. In this phenomenon concentration profiles decline as illustrated in Fig. 9.

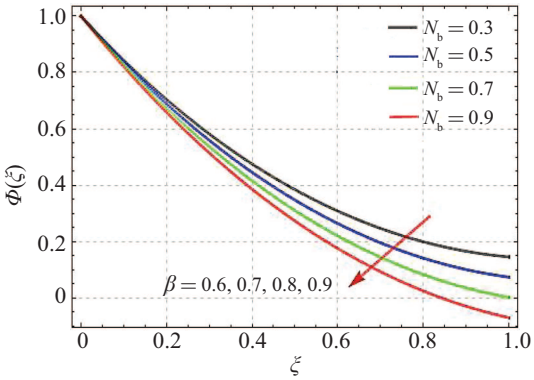


Fig. 9. Concentration curves for different values of β and N_b.

Figure 10 shows the influence of Schmidt number S_c on concentration characteristic for $\beta = 0.4, 0.5, 0.6, 0.7$. It is seen from this figure that expansion in S_c causes retardation in concentration profiles. Essentially, S_c relates mass diffusivity to momentum diffusivity, hence greater values of S_c decline the mass diffusion for which a smaller amount of mass transportation occurs. Therefore, concentration profiles decline with progression in S_c.

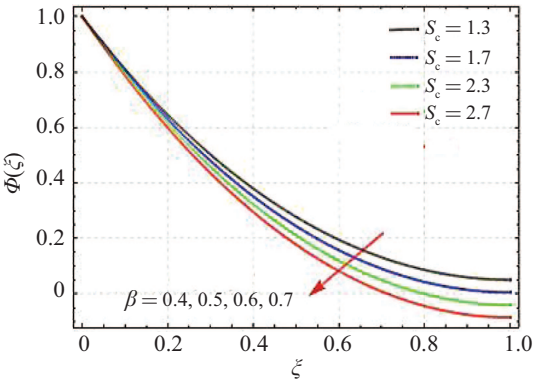


Fig. 10. Concentration curves for different values of β and S_c.

In Fig. 11 it can be seen that for Maxwell factor $\lambda_C = 1, 2, 3, 4$ and $\beta = 0.5, 5.2, 5.3, 5.4$ the concentration of fluid drops significantly. It can be explained by the fact that with the growing of λ_C less mass diffuses that declines the strength of boundary layer of concentration that justifies the retardation of concentration profiles. In Fig. 12 it can be seen that when $\beta = 0.6, 0.7, 0.8, 0.9$ the concentration of Maxwell nanofluid

augments for the increase of N_t. Basically, for greater values of N_t maximum diffusion of mass occurs that augments concentration layer and ultimately increases concentration profiles as portrayed in Fig. 12.

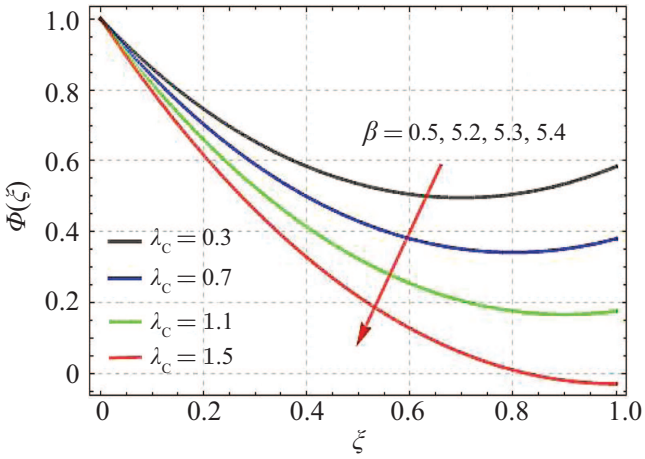


Fig. 11. Concentration curves for different values of β and λ_C.

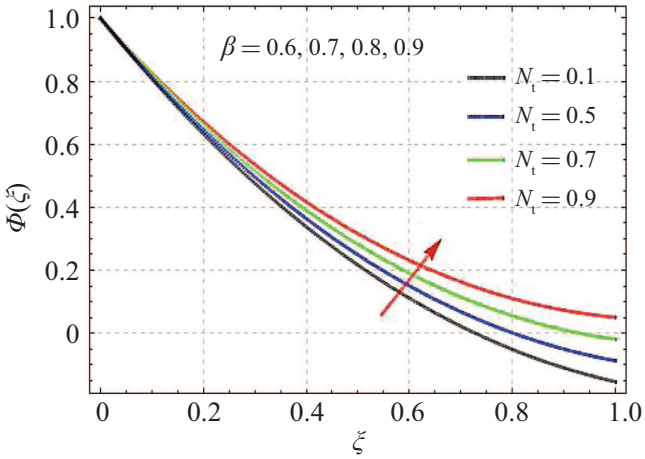


Fig. 12. Concentration curves for different values of β and N_t.

4.4. Analysis of entropy rate and Bejan number

The influences of various substantial factors on irreversibility rate and Bejan number are shown in Figs. 13–16.

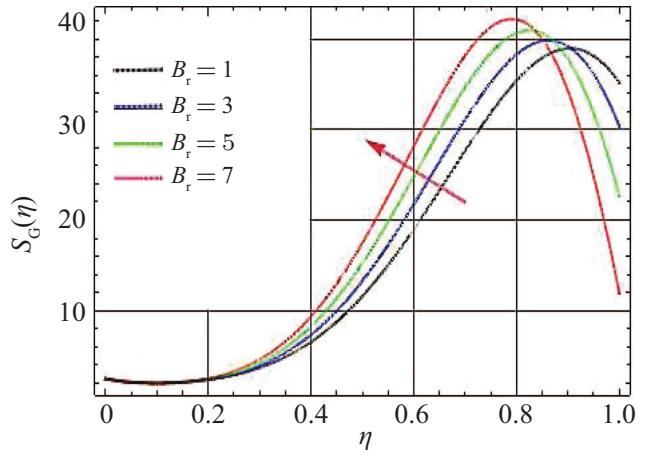


Fig. 13. Entropy rate curves for different values of B_r.

The effects of B_r (Brinkman number) on entropy and Bejan number are shown in Figs. 13 and 14. It is obvious that B_r controls the heat that is released in conduction of molecules through a relation of viscous heating to heat transportation. Further, the thermal conductivity of fluid decays with the growing of B_r, thereby upsurging the entropy as depicted in Fig. 13. In this phenomenon the value of Bejan number shrinks as presented in Fig. 14. For the larger values of thermal radiation factor the entropy of the fluid flow system upsurges due to converging internal energy into thermal energy as shown in Fig. 15. The Bejan number declines again with the value of R_d increasing as indicated in Fig. 16.

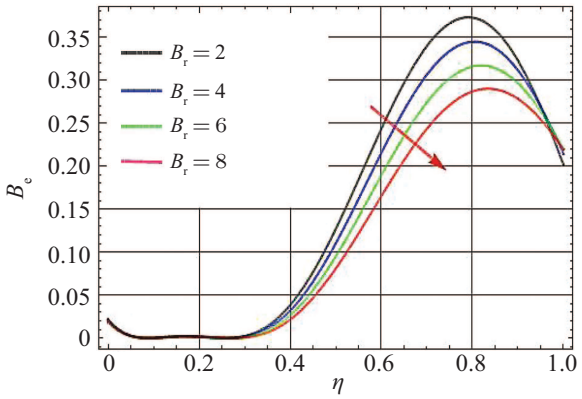


Fig. 14. Bejan number curves for different values of B_r.

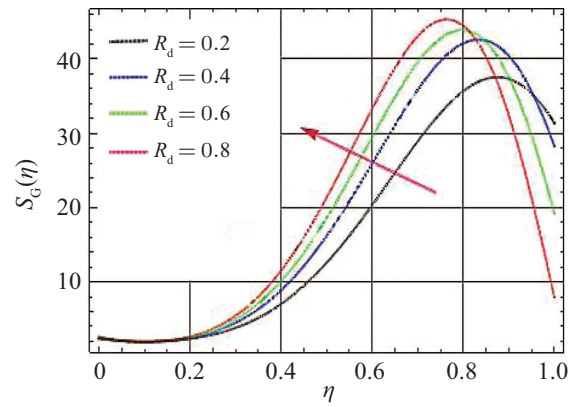


Fig. 15. Entropy rate curves for different values of R_d.

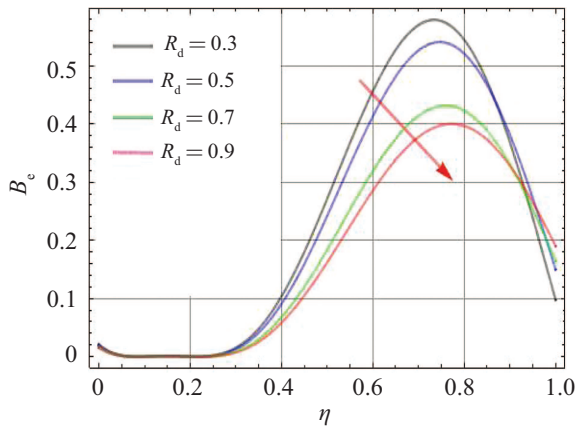


Fig. 16. The Bejan number curves for different values of R_d.

4.5. Discussion of tables

In the following Tables 1–3, the influence of different substantial factors upon important engineering quantities have been carried out.

Table 1. Numerical values of skin friction $Re^{1/2}C_f = f''(0)$.

λ	M	S	β	$f''(0)$
0.2	0.3	0.3	0.5	0.5242540
0.4				0.5376850
0.6				0.5489654
	0.5			0.5354320
	0.7			0.5431020
		0.5		0.5512032
		0.7		0.5610786
			0.55	0.5965320
			0.6	0.6565421

In Table 1, it has perceived that the skin friction has improved for the growth in magnetic, unsteadiness, and film thickness factors as these factors propose more resistance to the fluid velocity due to which maximum friction generated. Next as the thermal diffusivity rises with upsurge in the Brownian motion, unsteadiness and thermophoresis factors while decays for growth in thickness of film and Maxwell factor. Therefore, the Nusselt number supplements for augmentation in unsteadiness, Brownian, and thermophoresis factors and lower values of the film thickness and Maxwell factor as given in Table 2.

Table 2. Mathematical data for Nusselt number $Re^{1/2}N_u = -\Theta'(0)$.

N_t	S	λ_T	N_b	$-\Theta'(0)$
0.2	0.3	0.3	0.1	5.35231020
0.4				5.36785421
0.6				5.37802282
	0.5			5.29367500
	0.7			5.25653000
		1.5		5.33023100
		2		5.32087567
			0.3	5.37642200
			0.5	5.38754220

Table 3. Numerical values of Sherwood number $Re^{1/2}Sh_u = -\Phi'(0)$.

S_c	N_b	S	N_t	$-\Phi'(0)$
1.5	0.1	0.1	0.1	6.234012
2.5				6.193201
3.5				6.1302341
	0.3			6.3245532
	0.5			6.310321
		0.3		6.180231
		0.5		6.1265804
			0.3	6.2808528
			0.5	6.27021643

It has noticed in Table 3 that Sherwood number grows up for higher values of thermophoretic factor and retards with growth in Schmidt number, Brownian and Maxwell factors. In Tables 4 and 5 comparison between the established work (Qasim *et al.*[1]) and present work has conducted with a good agreement among both results.

Table 4. Comparison of common factors regarding Nusselt number between present results and previous results by Qasim *et al.*[1]

Common parameter	Qasim *et al.*[1]	Qasim *et al.*[1]	Present	Present
S	$\Theta(\beta)$	$-\beta\Theta'(0)$	$\Theta(\beta)$	$-\beta\Theta'(0)$
0.3	0.45921	0.64374	0.45963	0.64488
0.7	0.47941	0.768321	0.47972	0.769413
1.1	0.49916	0.853872	0.49973	0.856210
1.5	0.51732	0.88182	0.51821	0.883021

Table 5. Comparison of common factors regarding Sherwood number between present results and previous results by Qasim *et al.*[1]

Common parameter	Qasim *et al.*[1]	Qasim *et al.*[1]	Present	Present
S_c	$\Phi(\beta)$	$-\Phi'(0)$	$\Phi(\beta)$	$-\Phi'(0)$
8	0.53210	0.89310	0.53332	0.89421
9	0.412098	0.753201	0.414201	0.75433
10	0.312804	0.63264	0.314216	0.634205

5. Conclusions

This work explores the impact of double diffusion over thermally radiative flow of thin film hybrid nanofluid through a stretching channel. The nanoparticles of Ag and TiO_2 have been mixed in the base fluid taken as Maxwell fluid. Magnetic field influence has been employed to the flow system. The equations that are going to administer the fluid flow have been converted to dimension-free form by employing suitable set of variables. The impact of different substantial factors upon flow profiles has been discussed in detail. Some conclusions can be drawn from the present study below.

(i) Velocity profiles have been reduced with growth in film thickness factor and unsteadiness parameter as both factors have adverse effects upon fluid motion.

(ii) Growing values of magnetic factor yields Lorentz force in reverse direction of motion of fluid for which fluid particles experienced a resistance and ultimately decline the motion of fluid.

(iii) Temperature profiles have been augmented with upsurge in thermophoresis, unsteadiness parameters and Brownian motion factor for rising values of film thickness.

(iv) Temperature profiles have declined with progression in the values of film thickness and thermal Maxwell factor.

(v) Concentration has retarded with advancement in Schmidt number, Brownian motion, and concentration Maxwell factors.

(vi) For greater values of thermophoresis factor, maximum diffusion of mass occurs, which augments concentration layer and ultimately increases concentration profiles.

(vii) With the increase of Brinkman number and radiation factor, the irreversibility rate grows up while Bejan number declines.

(viii) The values listed in the tables show that for $\lambda = 0.2$, 0.4, 0.6; $M = 0.3$, 0.5, 0.7; $S = 0.3$, 0.5, 0.7; and $\beta = 0.5$, 0.55, 0.6 to 0.6, the skin friction of Maxwell nanofluid increases from 0.524254 to 0.6565421.

(ix) For $N_t = 0.2$, 0.4, 0.6, $S = 0.3$, 0.5, 0.7, $\lambda_t = 0.3$, 1.5, 2.0, and $N_b = 0.1$, 0.3, 0.5, the Nusselt number varies from 5.3523102 to 5.3875422, which depicts an augmentation in Nusselt number.

(x) For $S_c = 1.5$, 2.5, 3.5, $N_b = 0.1$, 0.3, 0.5, $S = 0.1$, 0.3, 0.5, and $N_t = 0.1$, 0.3, 0.5, the Sherwood number varies from 6.2340120 to 6.27021643, which shows an augmentation in mass diffusivity.

(xi) The results of this investigation have compared with published results, showing that they are in good agreement with the previous results.

References

[1] Qasim M, Khan Z H, Lopez R J and Khan W A 2016 *Eur. Phys. J. Plus* **131** 1
[2] Adebayo I, Xie Z, Che Z and Matar O K 2017 *Phys.l Rev. E* **96** 013118
[3] Akkuş Y, Tarman H I, Çetin B and Dursunkaya Z 2017 *Int. J. Therm. Sci.* **121** 237
[4] Dandapat B S, Singh S K and Maity S 2017 *Int. J. Mech. Sci.* **130** 367
[5] Saeed A, Kumam P, Nasir S, Gul T and Kumam W 2021 *Sci. Rep.* **11** 1
[6] Islam S, Khan A, Kumam P, Alrabaiah H, Shah Z, Khan W, Zubair M and Jawad M 2020 *Sci. Rep.* **10** 17823
[7] Nadeem S, Haq R U and Khan Z H 2014 *J. Taiwan Inst. Chem. Eng.* **45** 121
[8] Zainal N A, Nazar R, Naganthran K and Pop I 2021 *Appl. Math. Mech.* **42** 1511
[9] Jawad M, Saeed A, Khan A, Ali I, Alrabaiah, H, Gul T, Bonyah E and Zubair M 2021 *AIP Adv.* **11** 035215
[10] Abdal S, Siddique I, Alrowaili D, Al-Mdallal Q and Hussain S 2022 *Sci. Rep.* **12** 278
[11] Abbasi F M and Shehzad S A 2016 *J. Mol. Liq.* **220** 848
[12] Rashidi S, Esfahani J A and Maskaniyan M 2017 *J. Magn. Magn. Mater.* **439** 358
[13] Turkyilmazoglu M 2022 *Zeitschrift für Naturforschung A* **77** 329
[14] Saleh H and Hashim I 2010 *Chin. Phys. Lett.* **27** 024401
[15] Fan J Y, Feng Y, Lu D, Zhang W C, Hu D Z, Yang Y E, Tang R J, Hong B, Ling L S, Wang C X, Ma C L and Zhu Y 2019 *Acta Phys. Sin.* **68** 107501 (in Chinese)
[16] Uddin I, Ullah I, Raja M A Z, Shoaib M, Islam S, Zobaer M S, Nisar K S, Saleel C A and Alshahrani S 2021 *Sci. Rep.* **11** 19239
[17] Hosseinzadeh K, Mardani M R, Salehi S, Paikar M and Ganji D D 2021 *Pramana* **95** 57
[18] Guedri K, Khan A, Gul T, Mukhtar S, Alghamdi W, Yassen M F and Tag Eldin E 2022 *ACS Omega* **7** 33432
[19] Choi S U and Eastman J A 1995 "Enhancing thermal conductivity of fluids with nanoparticles" (No. ANL/MSD/CP-84938; CONF-951135-29), Argonne National Laboratory (ANL), Argonne, IL (USA)
[20] Najafabadi M F, TalebiRostami H, Hosseinzadeh K and Ganji D D 2022 *Theor. Appl. Mech. Lett.* **12** 100356
[21] Ghadikolaei S S, Hosseinzadeh K, Ganji D D and Jafari B 2018 *Case Studies in Thermal Engineering* **12** 176
[22] Shah Z, Khan A, Khan W, Alam M K, Islam S, Kumam P and Thounthong P 2020 *Computer Methods and Programs in Biomedicine* **186** 105197
[23] Khan A, Saeed A, Gul T, Mukhtar S, Ali I and Jawad M 2021 *Physica Scripta* **96** 045206
[24] Bilal M, Ahmed A E S, El-Nabulsi R A, Ahammad N A, Alharbi K A M, Elkotb M A, Anukool W and Sa Z A 2022 *Micromachines* **13** 874
[25] Rajput N S, Shukla D D, Ishan L and Madhav K S 2021 *Materials Today: Proceedings* **47** 6508
[26] Ullah H, Hayat T, Ahmad S and Alhodaly M S 2021 *Int. Commun. Heat Mass Transfer* **122** 105111
[27] Butt A S and Ali A 2013 *Chin. Phys. Lett.* **30** 024701
[28] Cheng X T and Liang X G 2013 *Chin. Phys. B* **22** 080509
[29] Khan A, Shah Z, Alzahrani E and Islam S 2020 *Int. Commun. Heat Mass Transfer* **119** 104979
[30] Liao S J 1999 *Int. J. Nonlinear Mech.* **34** 759
[31] Gul T, Mukhtar S, Alghamdi W, Ali I, Saeed A and Kumam P 2022 *ACS Omega* **7** 33365
[32] Khan A, Hassan B, Ashraf E E and Shah S Y A 2022 *Heat Transfer* **51** 1170